

Supplementary Information Appendix for

Structural basis for *Acinetobacter baumannii* biofilm formation

Natalia Pakharukova, Minna Tuittila, Sari Paavilainen, Henri Malmi, Olena Parilova, Susann Teneberg, Stefan D. Knight and Anton V. Zavialov*

correspondence to: antzav@utu.fi

This PDF file includes:

<i>SI</i> Materials and Methods	pages 2-3
Figs. S1 to S14	pages 4-21
Tables S1 to S3	pages 22-24
<i>SI</i> References	page 25

SI Materials and Methods

Bacterial strains and plasmids. Characteristics and source of the bacterial strains used in this study are given in Supplementary Table S1. Oligonucleotides are listed in Supplementary Table S2.

The *Csu* gene cluster was amplified by PCR from chromosomal DNA of *Acinetobacter baumannii* Bouvet and Grimont (ATCC® 19606D-5™) using primers CsABABCDE_N-F and CsABABCDE_S-R. The PCR product was digested with restriction enzymes *Not*I and *Sac*I and cloned in *Sac*I-*Not*I digested pBAD-ENSPA downstream the P_{BAD} promoter (1). The resulted plasmid was named as pBAD-Csu. Deletions of genes of the Csua/B, Csua, Csub, and Csue subunit in pBAD-ABABCDE were constructed by reverse PCR using oligonucleotides Δ-CsuaB-R and -F, Δ-Csua-R and -F, Δ-Csub-R and -F and Δ-Csue-R and -F, respectively. Replacements of residues 40-43 (LALA) to SGSG (L₄₀ALA₄₃→SGSG), 140-145 (IVGIGV) to SSGSGS (I₁₄₀VGIGV₁₄₅→SSGSGS), 157-159 (LGI) to SGS (L₁₅₇GI₁₅₉→SGS) in Csue were generated by reverse PCR and oligonucleotides Csue-LALA_R and -_F, Csue-IVGIGV_R and -_F and Csue-LGI_R, respectively. The L₄₀ALA₄₃→SG mutation was introduced by accident, as a side product of the PCR intended to introduce the L₄₀ALA₄₃→SGSG mutation.

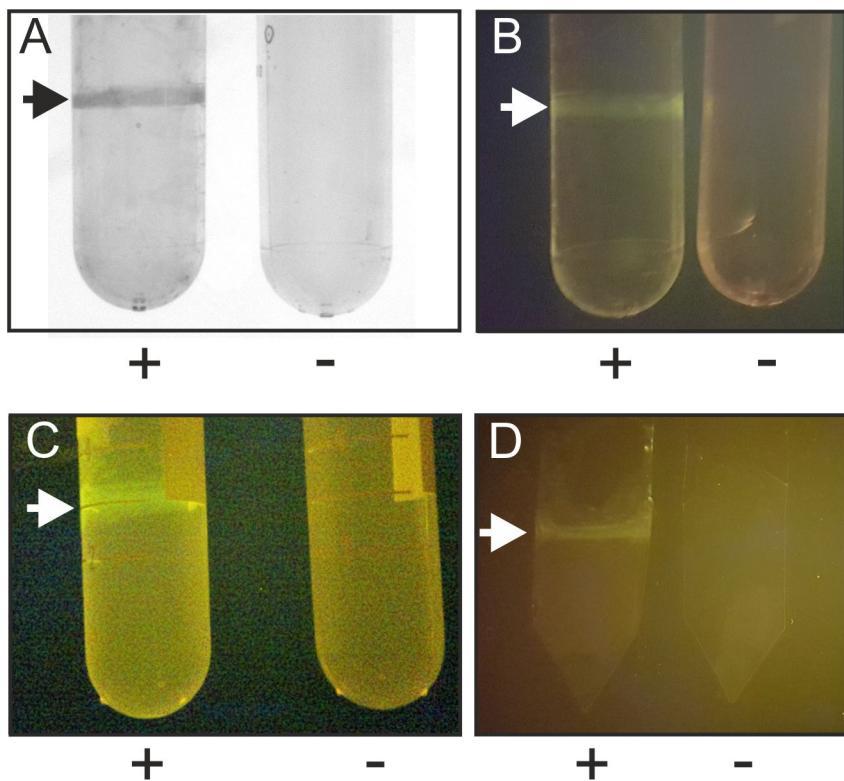
To express isolated N-terminal domain of Csue (Csue_{NTD}), synthetic nucleotide sequence encoding the first 205 residues of Csue including the secretion sequence peptide was ordered from GenScript and inserted downstream of the T7 promoter in the pET101D expression vector (Invitrogen). To facilitate the purification of the domain a C-terminal His tag was added to the expression plasmid using reverted PCR and primers CsueN6Hrev and CsueN6Hfwd. To improve the protein stability and increase the level of expression, codons for Pro206 and Asp207 were introduced preceding the His tag coding region by reverse PCR using primers Csue-N6H_PR and Csue-N6H_DF. The resulting plasmid was termed pET101-CsuE-NPD6H.

To generate the I₁₄₀VGIGV₁₄₅→SSGSGS mutation in Csue_{NTD} and Csue co-expressed with Csuc, plasmids pET101-CsuE-NPD6H and pET101-CsuC6H-CsuE, respectively, were amplified using oligonucleotides Csue-IVGIGV_R and Csue-IVGIGV_F. The PCR products were blunt-end ligated, resulting in expression plasmids pET101-CsuE-NPD6H-SSGSGS and pET101-CsuC6H-CsuE-SSGSGS.

Analysis of CsuE binding to plastics. Wild type and I₁₄₀VGIGV₁₄₅→SSGSGS mutant CsuE complexed with the CsuC chaperone were purified essentially as described in (2). To enable detection of the protein by measuring time-resolved fluorescence, purified complexes were labeled with Eu⁺³-chelate. 65 μM complex was incubated with 194 μM Kajo615 Eu⁺³-chelate (Kaivogen) in 88.6 mM bicarbonate buffer, pH 9.8 at 4°C for 18 h. The reaction was stopped by adding 20 μl 3.0 M Tris-HCl, pH 8.45. Labeled proteins were kept on ice until gel filtration on a Superdex75 10/300 GL column (GE Healthcare) equilibrated with 50 mM Tris-HCl (pH 7.5) and 150 mM NaCl (buffer A). Eluted proteins were concentrated on a Vivaspin device with 5 kDa molecular weight cut off (GE Healthcare). Protein concentration was measured using a NanoDrop 2000 spectrophotometer (Thermo Scientific).

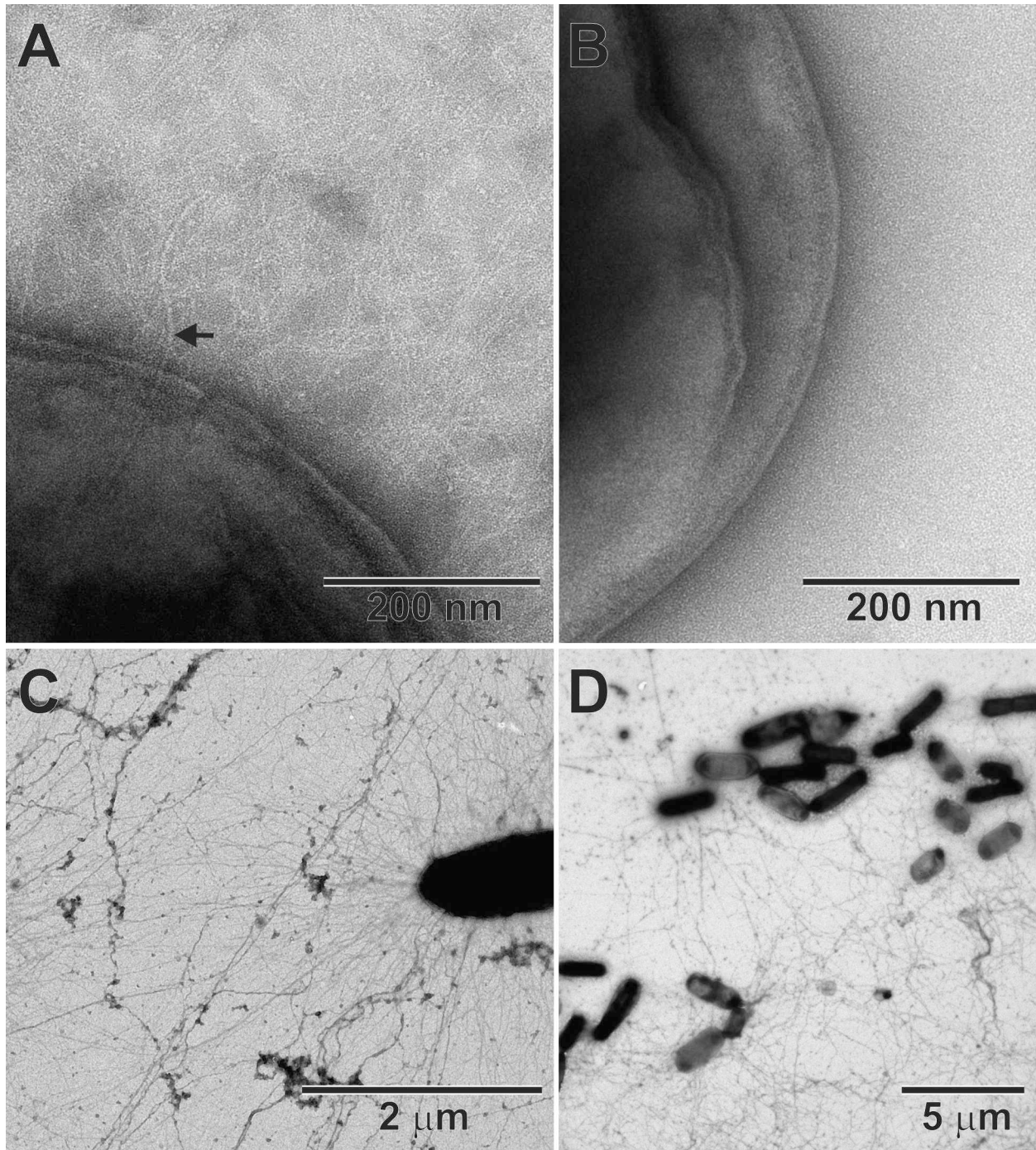
To ensure the comparability of the wild type and mutant binding experiments, the two were measured simultaneously, side-by-side. Labeled complexes (60 μg/ml in buffer A) were first incubated on ice in a 2 ml polypropylene tube (Sarstedt) for 30 min to ensure that the concentration is no longer changed due to binding to the plastic tube. 1 ml of the wild type and mutant proteins were pipetted simultaneously onto two 5.5 cm Petri dishes (Sarstedt) and shaken horizontally by hand to ensure the volume covered the entire bottom surface of the dishes. The binding experiment was done at 22°C with 250 rpm shaking on an automatic shaker (New Brunswick Scientific) to maintain uniformity of the sample volume. 7.2 μl samples were withdrawn at different time points and added into wells of a SpectraPlate™-96HB (PerkinElmer) plate for measuring Eu⁺³ fluorescence. To estimate the initial concentration of the complex (0 time point of the reaction), 7.2 μl of the protein was taken for the fluorescence measurement directly from the tube. The samples were mixed for 10 to 15 min with 140 μl of Europium Fluorescence Intensifier (Kaivogen). As the fluorescence signal was very high, each sample was divided after mixing into three wells and the sum of signals from the three wells was used as the signal value. The delayed fluorescence was measured using a Victor3 1420 multi-label counter (PerkinElmer). The binding curves were corrected for evaporation from the plate. The evaporation effect was estimated by measuring the change in fluorescence of an unreactive form of the Kajo615 label incubated on a Petri dish in 1 ml buffer A, containing 1.94 pM BSA.

Fig. S1.



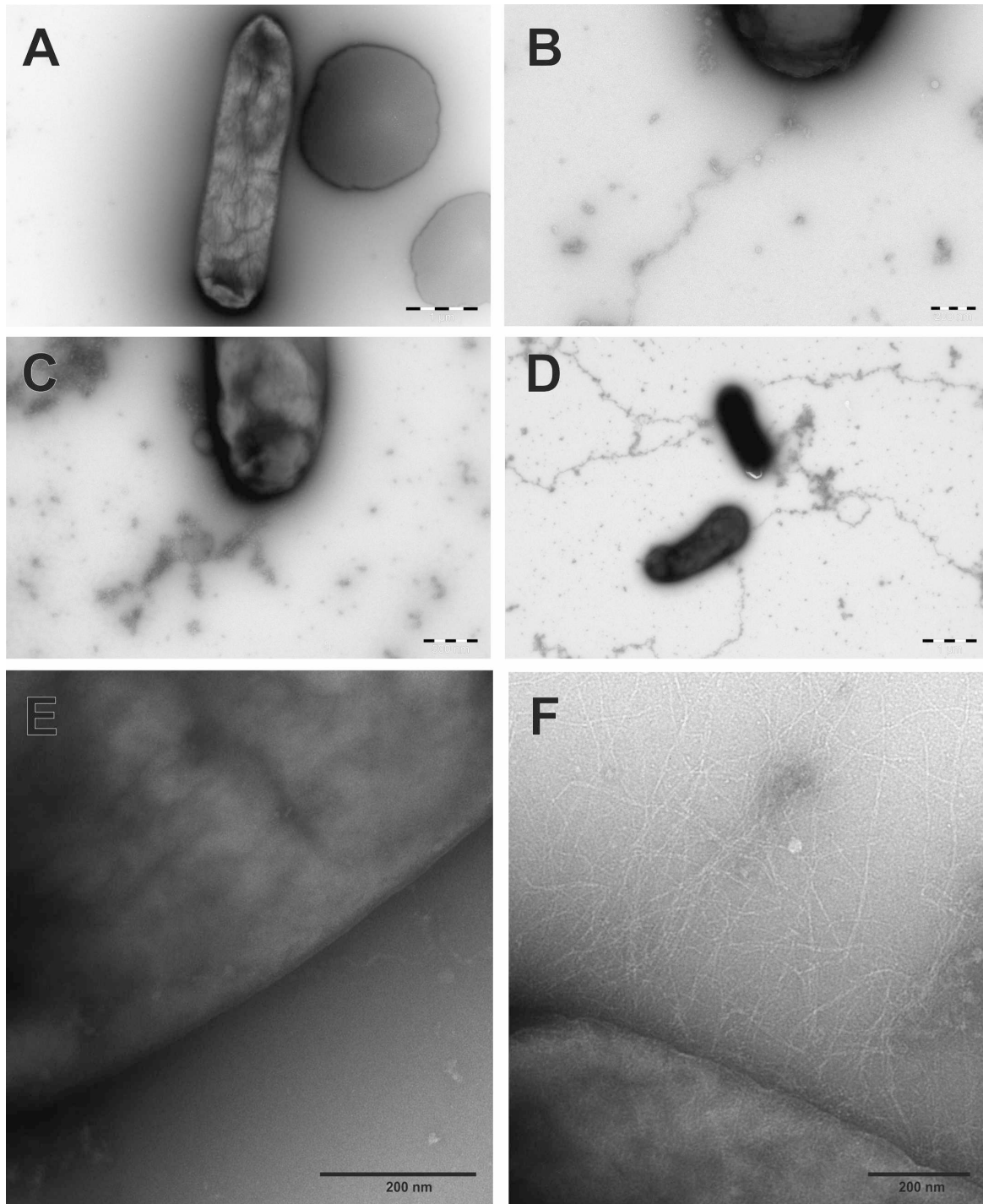
Csu pili mediate biofilm formation of recombinant *Escherichia coli* on abiotic surfaces. Cs_U pili expression was induced (+) or not induced (-) in *E. coli* harboring pBAD-Cs_U and pYFP plasmids. Bacterial cells were incubated in polystyrene (**A** and **B**) and polypropylene (**C**) tubes for 6 h at 37°C in LB medium. Attached cells were detected by staining with crystal violet (**A**) or by observation of fluorescence owing to the expression of yellow fluorescence protein (**B** and **C**). To study binding to the hydrophilic surface of cellophane (**D**), straps of cellophane were added to the tubes and incubated with bacteria expressing or not expressing Cs_U pili, gently washed and analyzed as in (**B**) or (**C**). Although biofilm was observed on hydrophilic cellophane (**D**), cells were detached from these surfaces much more easily than from hydrophobic polystyrene, polypropylene or polyethylene surfaces.

Fig. S2



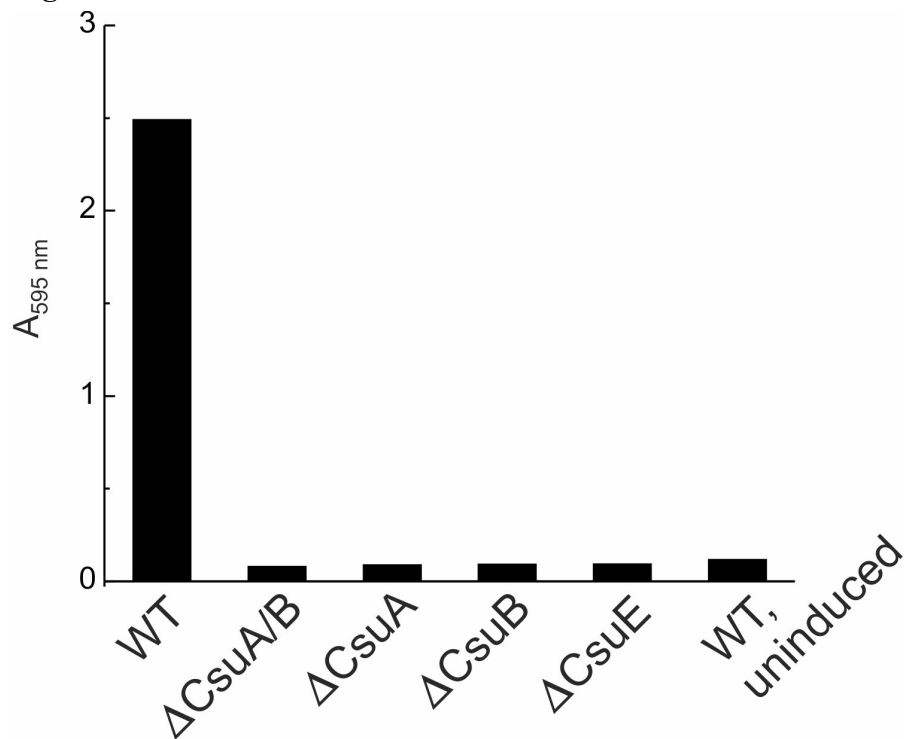
Representative transmission electron microscopy micrographs of *E. coli* expressing CsU pili.
E. coli strain BL21 harboring the pBAD-ABABCDE plasmid was cultured in LB medium in presence (**A, C** and **D**) or absence (**B**) of arabinose and stained with ammonium molybdate. Micrographs of different magnification are shown. The arrow in **A** indicates an individual pilus clearly seen on the image. The CsU pilus is about 3.5 nm in diameter and is typically 1-2 μm long. However, some pili can reach 5 μm in length (3-6 times longer than the prototypical classical type 1 and P pili) and form long bundles well visible in (**D**).

Fig. S3



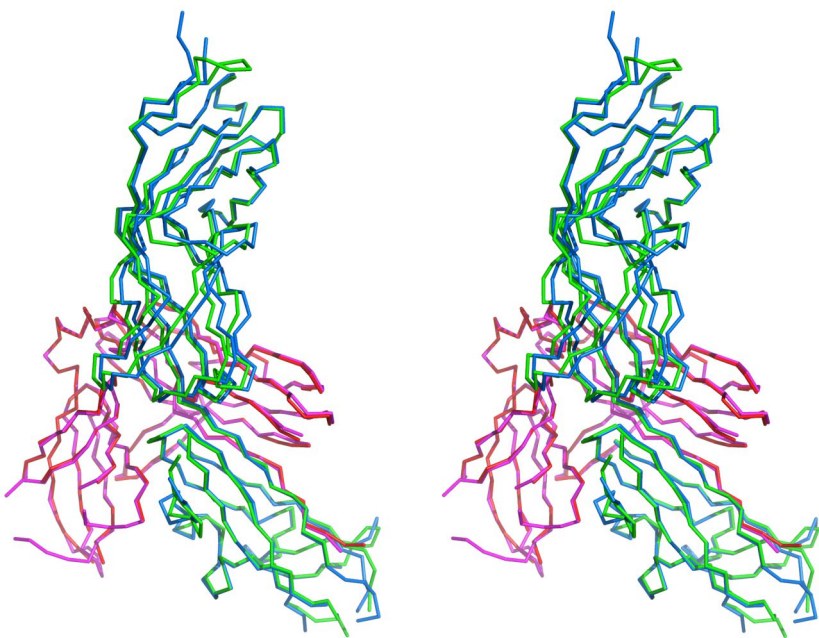
Effect of mutations on Csu pilus expression. *E. coli* harboring pBAD-ABABCDE derivatives, carrying deletions of entire genes of CsuA/B (**A**), CsuA (**B**), CsuB (**C** and **D**), CsuE (**E**) or a substitution of residues 140-145 in CsuE with SSGSGS ($I_{140}VGIGV_{145} \rightarrow SSGSGS$, **F**), were cultured in LB medium in the presence of arabinose and stained with ammonium molybdate. Deletion of genes coding for CsuA/B and CsuE completely abolished the pilus assembly. Δ CsuA and Δ CsuB mutants expressed a few thick and long pili (**B-D**). The $I_{140}VGIGV_{145} \rightarrow SSGSGS$ mutation did not affect pilus assembly (**F**).

Fig. S4



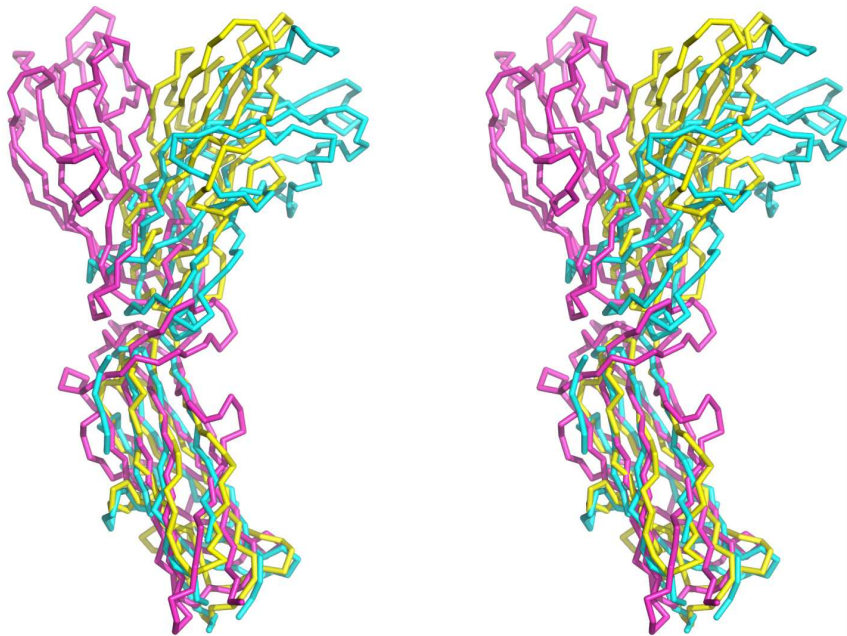
Quantification of biofilms of *E. coli* harboring the wild type and subunit deleted *Csu* gene cluster. An entire gene of CsuA/B, CsuA, CsuB or CsuE subunit was deleted (Δ) from the *Csu* gene cluster. Arabinose was added to induce pilus expression. Uninduced wild type (WT) cells were used as a negative control. Biofilms were stained with crystal violet, processed as described in Materials and Methods, and quantified by measuring absorbance at 595 nm.

Fig. S5



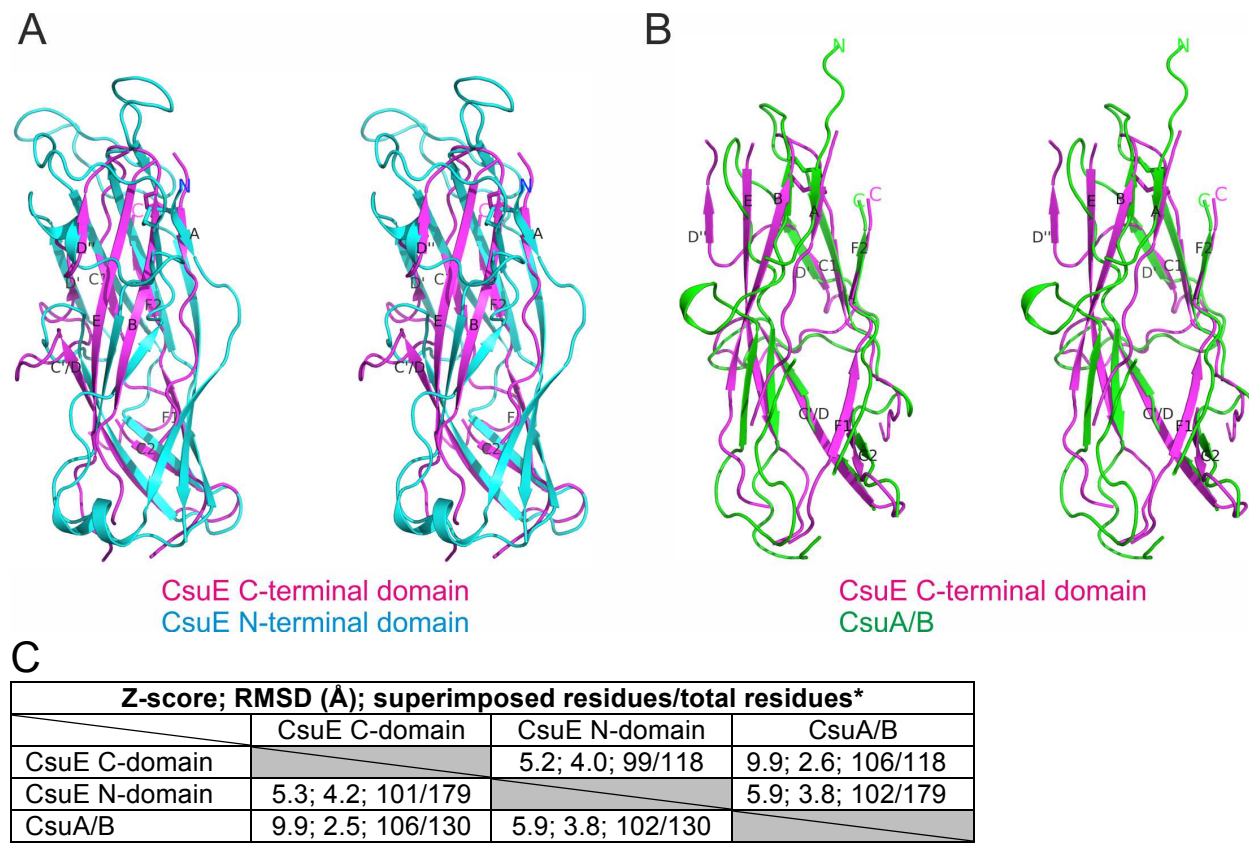
Structural comparison of two copies of CsuC-CsxE in the asymmetric unit. Molecules were superimposed by distance minimization between C α atoms of CsuC. CsuC and CsxE are colored red and green in one complex and magenta and marine in another complex, respectively. Note that major differences are observed in the region of the N-terminal domain of CsxE. Most of these differences are caused by a change in the angle between domains in CsxE.

Fig. S6



The angle between N- and C-terminal domains in CsxE is sharper than that in two-domain adhesin subunits from the classical (FimH) and alternative (CfaE) CU systems. CsxE (cyan), FimH (yellow), and CfaE (magenta) were superimposed by minimizing distances between C α atoms in β -strands of their C-terminal, adaptor (pilin) domains. Stereo pairs of C α -traces are shown. The angles between domains in CsxE, FimH, and CfaE are $\sim 135^\circ$, 150° , and 180° , respectively, as measured from the center of gravity of each domain to that of the connector. The shape of CsxE is closer to that of the FimH adhesin from classical type 1 pili. The angle between domains in FimH ($\sim 150^\circ$) has been suggested to be a part of mechanism for shear-force-enhanced attachment to receptors (5).

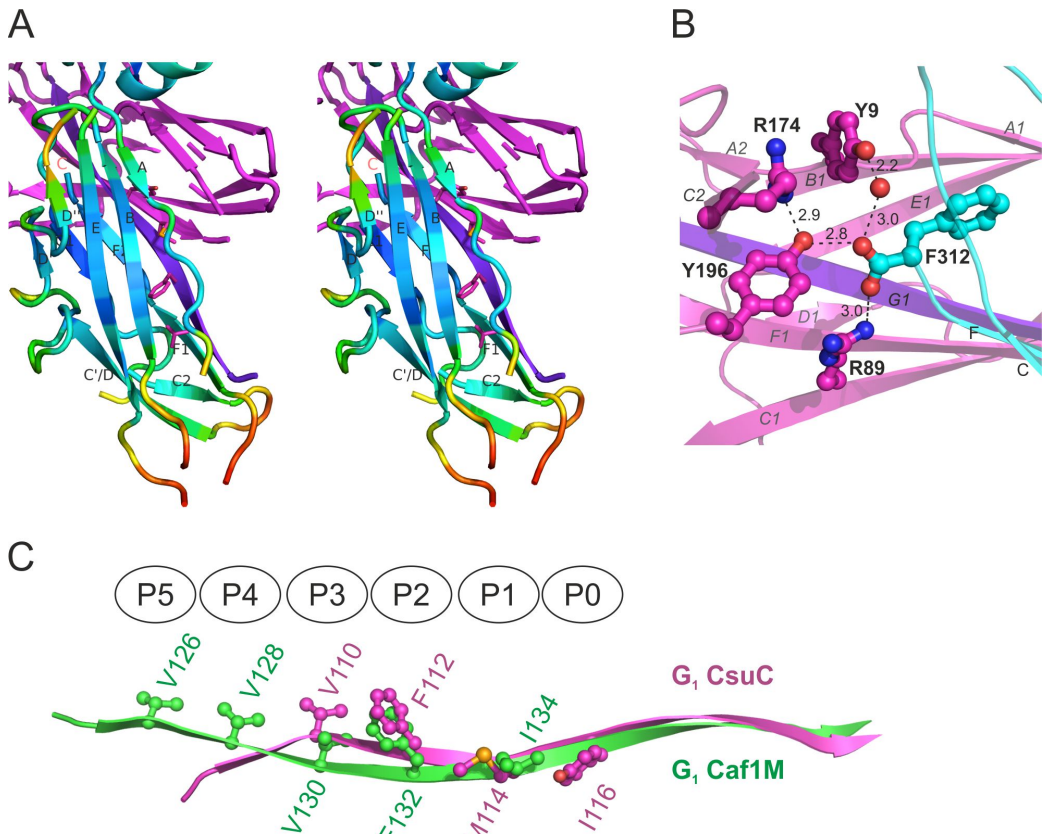
Fig. S7



*Total residues of protein shown in the column

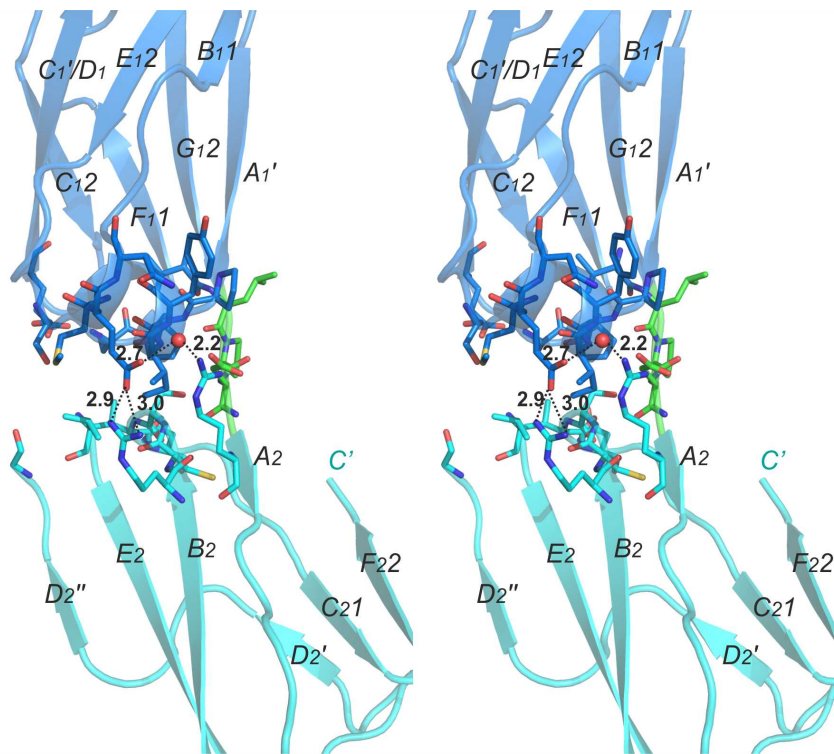
Structural comparison of C- and N-terminal domains of Csue between each other and the major Csua/b pilus subunit of Csue pili. (A and B) Cartoon diagrams of superpositions (stereo views) of C- (magenta) and N-terminal (cyan) domains of Csue (A) and C-terminal domain of Csue (magenta) and Csua/b (green) (B). Disulfide bonds are shown as stick models. Secondary structure elements in the C-terminal domain of Csue are labeled. Csuepd and Csua/b have a very different structure of β-sheet 1, ABED (B). In Csua/b, β-sheet 1 is split in the middle due to the loop insertions that interrupt its β-strands as in most CU subunits (6). In contrast, β-sheet 1 in Csuepd is uninterrupted, making the structure of Csuepd more similar to the canonical Ig-like fold of the 8-stranded h-type (7). Consistent with the h-type fold, strand D switches sheets, but then repeats this twice. Csue_{NTD} and Csuepd share a highly conserved disulfide bond connecting strands A and B (Fig. S11), but the structures of these domains differ substantially, and Csue_{NTD} is structurally distant from major pilin Csua/b. (C) Structural comparison statistics. Superpositions and statistics were generated with the DALI Lite server (http://ekhidna.biocenter.helsinki.fi/dali_lite/start) (8).

Fig. S8



Structure of the CsuC-CsxE complex highlights the characteristic features of non-classical assembly. (A) Chaperone-bound pilin domain (CsxEpd) has a large fraction of disordered or poorly ordered sequence. Close-up of the CsuC-CsxE structure, showing the structure of CsxEpd (cartoon diagram, stereo view). CsxE is colored by B-factor of Cα atoms with the color ranging from blue to red and corresponds to a B-factor range from 20 to 135 Å². CsuC is shown in magenta except for β-strand G1, which is violet. Donor strand residues are shown as sticks. Note the missing loops and elevated B-factors in the structure of CsxEpd distant from CsuC. (B) CsuC uses both domains to anchor the C-terminal carboxylate of CsxE rather than one as in the classical chaperones. Close-up of the CsuC-CsxA/B structure, demonstrating interactions between C-terminal carboxylate of CsxE and CsuC (cartoon diagram). The complex is painted as in Fig. 2. C-terminal Phe312 in CsxE and Tyr9, Arg89, Tyr196, and Arg174 in CsuC are shown as ball-and-stick. Hydrogen bonds are shown with dashes and their length is indicated. Residues Tyr9 and Arg89 belong to domain 1, whereas residues Tyr196 and Arg174 belong to domain 2. Tyr9 binds to the carboxylate via a structured water molecule (red sphere). This previously unidentified contact is also present in the CsuC-CsxA/B complex (6). (C) The donor strand motif in CsuC in the CsuC-CsxE complex is shifted towards the end of the G₁ strand relative to that in classical chaperones. Fragment of the superposition of CsuC-CsxE and Caf1M-Caf1 complexes, showing the alignment of G₁ donor strands in CsuC and Caf1M. Hydrophobic donor residues are shown as ball-and-stick and labeled. Positions of hydrophobic pockets P0-P5 in subunit acceptor clefts (P0-P3 in CsxE and P1-P5 in Caf1) are shown schematically above the donor strands.

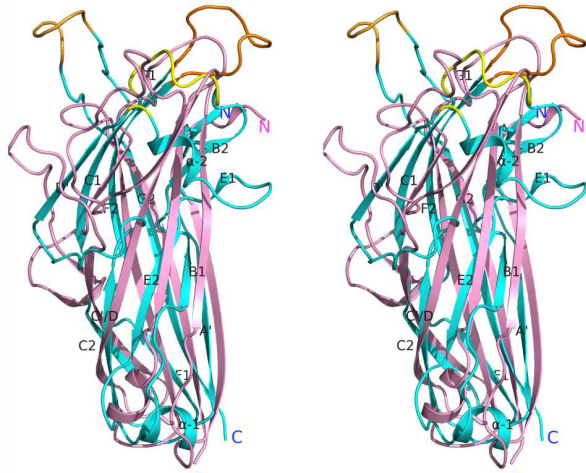
Fig. S9



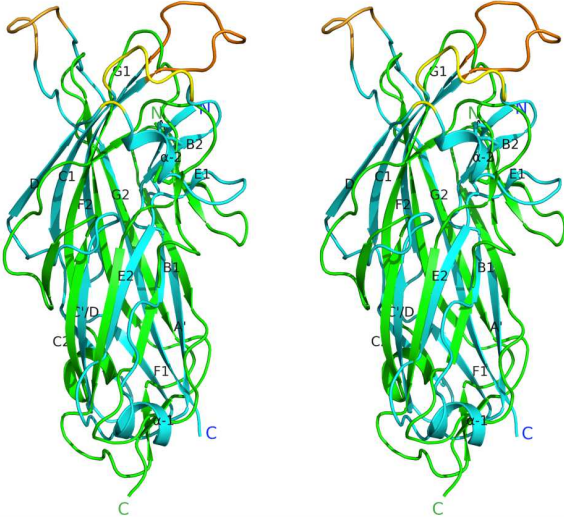
Cartoon diagram of CsxE illustrating the interface between N- and C-terminal domains (stereo view). N- and C-terminal domains are painted in blue and cyan, respectively. Residues engaged in interdomain contacts are shown as sticks. A structured water molecule participating in a network of hydrogen bonds between the two domains is shown as a red sphere. Hydrogen and ionic bonds are shown as dashed lines; the bond length is indicated. β -Strands and C-terminus are labeled. The buried area in CsxE (383 \AA^2) is only half of that in the CfaE subunit of CFA/I pili assembled via the alternative CU pathway, despite a similar size of the linker (9). This is explained by the striking difference in the angle between domains in these molecules (Fig. S6).

Fig. S10

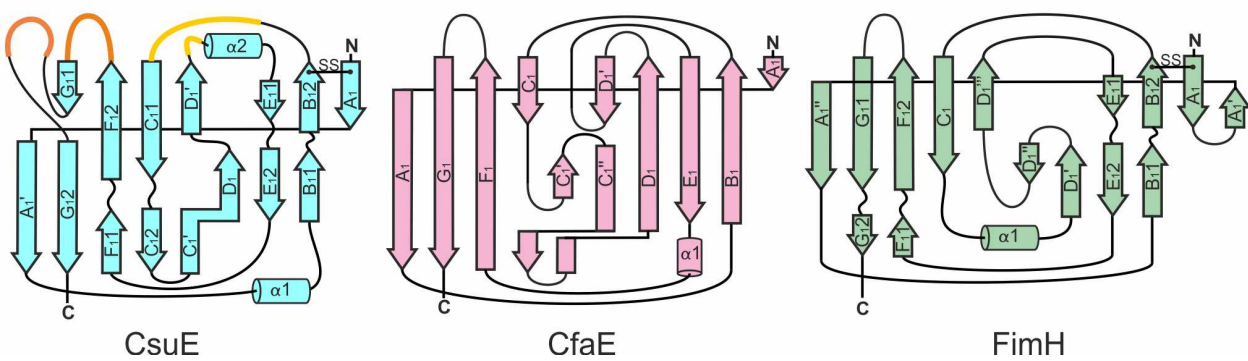
A



B



C



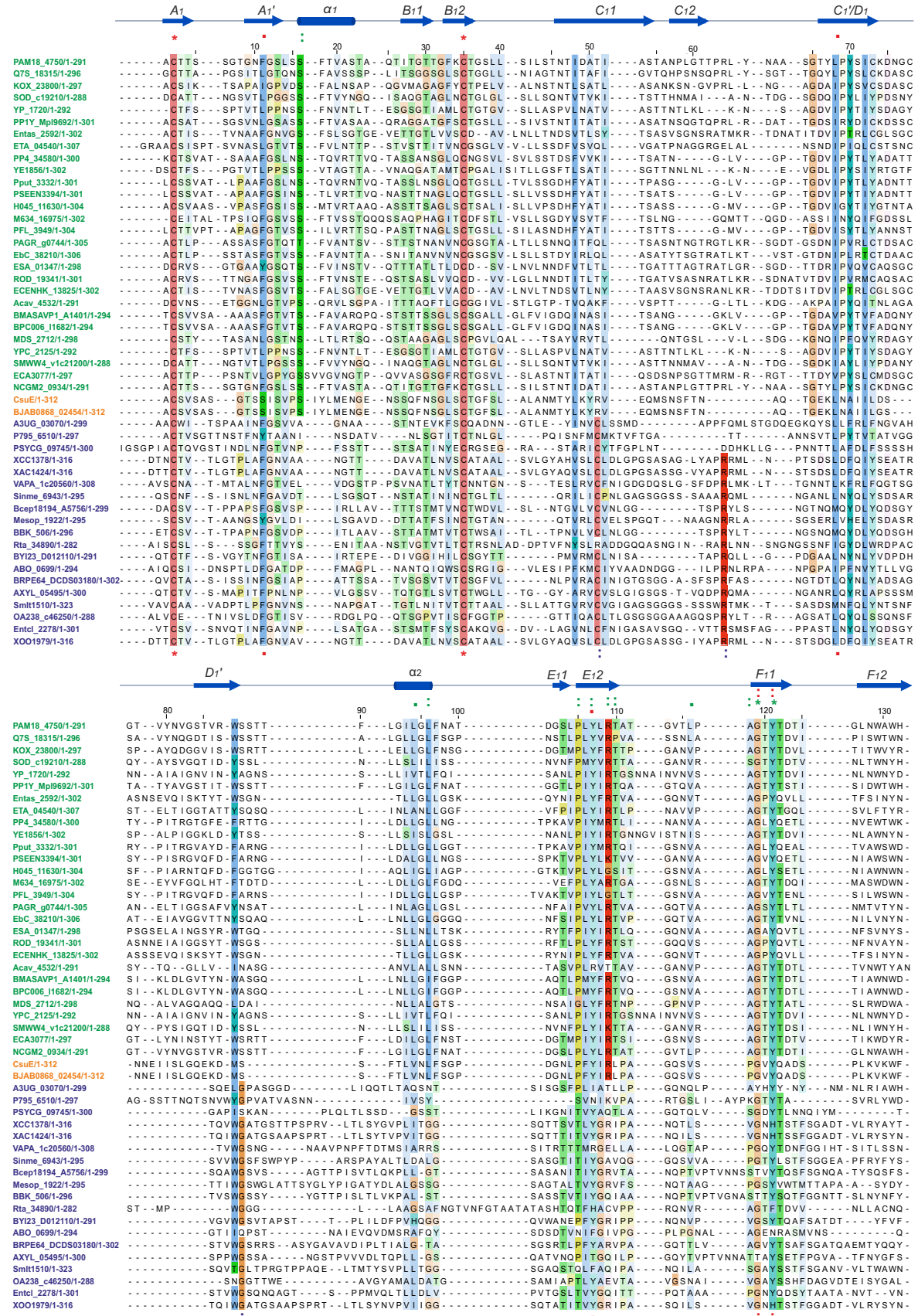
D

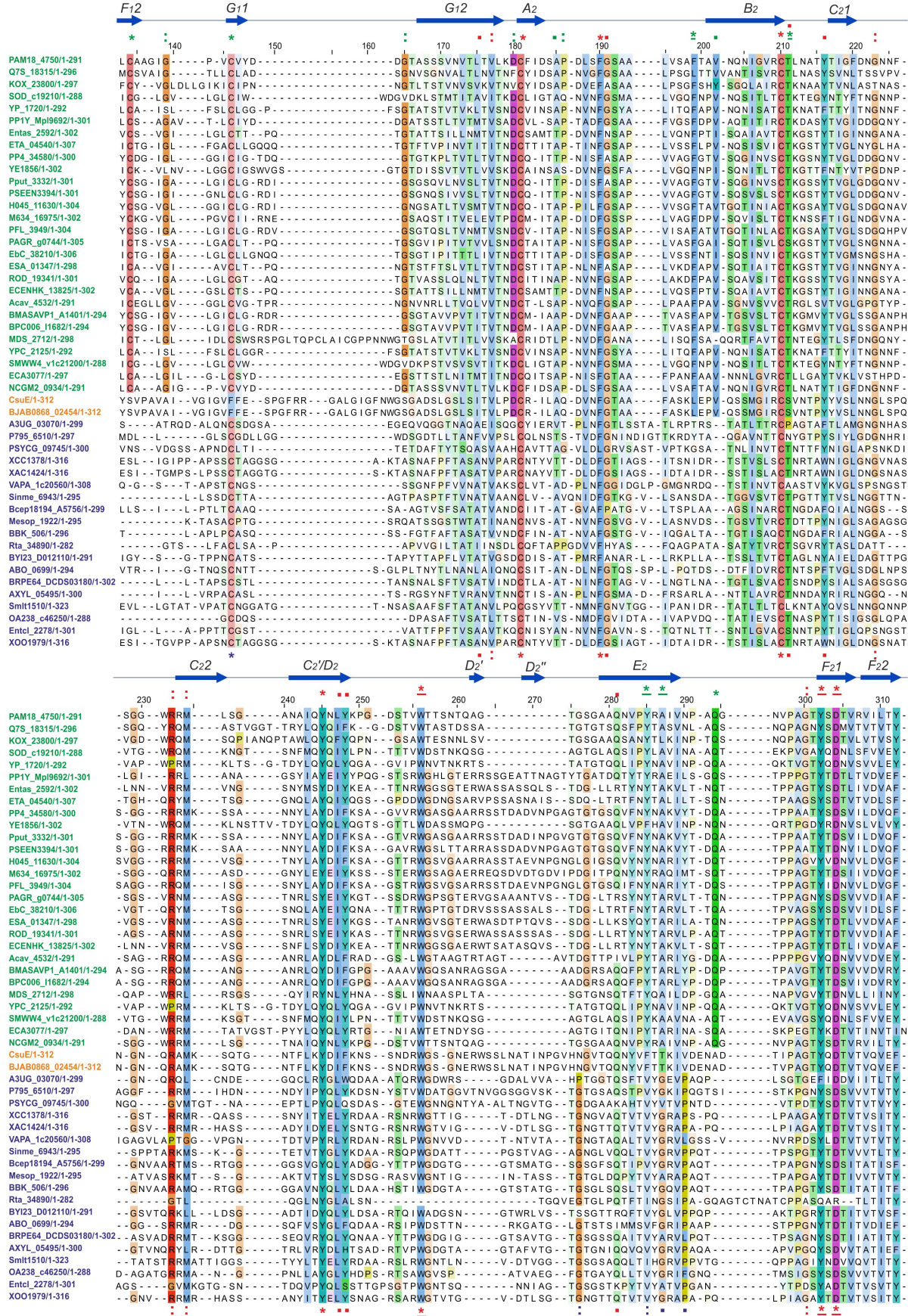
	CsuE N-domain	CfaE N-domain	FimH N-domain
CsuE N-domain		6.9; 3.2; 114/179	5.5; 3.7; 116/179
CfaE N-domain	6.9; 3.2; 114/178		4.5; 3.4; 98/178
FimH N-domain	5.5; 3.7; 116/158	4.5; 3.3; 98/158	

*Total residues of protein shown in the column

Structural comparison of N-terminal domains of CsuE, CfaE, and FimH. (A and B) Cartoon diagrams of superpositions (stereo views) of N-terminal domains of CsuE (cyan) and CfaE (pink) (A) and CsuE (cyan) and FimH (green) (B). Binding fingers 1-3 in CsuE are painted in yellow, orange, and light orange, respectively. Secondary structure elements in CsuE are labeled. Conserved disulfide bonds are shown as stick models. (C) Topology diagrams of CsuE, CfaE, and FimH. Strands and helices are shown as arrows and cylinders, respectively. (D) Structural comparison statistics.

Fig. S11





Alignment of two-domain tip subunits from archaic chaperone/usher (CU) systems. Sequences of two-domain subunits from archaic CU gene clusters were identified in various genomes (see the table bellow) and analyzed with the *SignalP 4.1* server to detect and exclude secretion signal peptides. The predicted mature sequences were aligned with the program Clustal Omega at the EMBL-EBI website (10). The aligned sequences were edited and annotated using the program JalView (11). Conserved residues are color-coded according to their chemical properties: blue — hydrophobic, green — hydrophilic neutral, red — basic, magenta — acidic. Conserved cysteine residues are colored in pink. Glycine residues are shaded in orange, proline in yellow, aromatic residues in cyan. The sequences of two-domain subunits fall into families: the first family occupies the top part of the alignment table, above *A. baumannii* CsxE, (names of these sequences are shown in green), and the second family occupies the bottom part of the alignment table, below *A. baumannii* BJAB0868_02454 (names of these sequences are shown in blue). Completely invariant residues are indicated with an asterisk (*) in red and conserved positions containing less than 4% variable residues with an underlined asterisk (*) in red. Highly conserved regions (up to 15% variable residues) are marked with double dots (:) in red. Residues essential for semi-conservation (up to 25% non-matching residues) are dotted (.) in red. Conserved residues within each of the two families are indicated in a similar way, but the corresponding symbols are shown in green and blue for family 1 and 2, respectively. Secondary structure of the *A. baumannii* strain 19606 CsxE subunit (this paper) is shown above the alignment. Blue arrows and bars denote β strands and α helices, respectively.

Sequence source

#	Subunit name	Operon	Usher Accession	Chaperone Accession	Subunits Accession	Organism	Organism Class	Associated Disease	Operon DNA Accession
1	PAM18_4750	PAM18_4745-4750	AEO77229.1	AEO77228.1	AEO77230.1 AEO77227.1 AEO77226.1 AEO77225.1	<i>Pseudomonas aeruginosa</i> M18	γ Proteobacteria	Isolated from sweet melon rhizosphere	CP002496
2	Q7S_18315	Q7S_18290-18315	AFE59873.1	AFE59872.1	AFE59874.1 AFE59871.1 AFE59870.1 AFE59869.1	<i>Rahnella aquatilis</i> HX2	γ Proteobacteria	Isolated from a vineyard soil	CP003403
3	KOX_23800	KOX_23780-23800	AEX06475.1	AEX06474.1	AEX06476.1 AEX06473.1 AEX06472.1	<i>Klebsiella oxytoca</i> KCTC 1686	γ Proteobacteria	Bacterium is used in production of 2,3-butylene glycol and 2,3-butanediol from xylose	CP003218
4	SOD_c19210	SOD_c19210-c19260	AGO54899.1	AGO54900.1	AGO54901.1 AGO54902.1 AGO54903.1 AGO54898.1	<i>Serratia plymuthica</i> 4Rx13	γ Proteobacteria	A plant-associated, plant beneficial bacterium	CP006250
5	YP_1720	YP_1720-1725	AAS61949.1	AAS61950.1	AAS61951.1 AAS61952.1 AAS61953.1 AAS61948.1	<i>Yersinia pestis</i> biovar <i>Microtus str. 91001</i>	γ Proteobacteria	Causative agent of bubonic and pneumonic plague	AE017042
6	PP1Y_Mpl962	PP1Y_Mpl9658-Mpl9692	CCA90809.1	CCA90808.1	CCA90807.1 CCA90806.1 CCA90810.1	<i>Novosphingobium</i> sp. <i>PP1Y Mpl</i> megaplasmid	α Proteobacteria	Isolated from a surface seawater sample collected from a closed bay	FR856861
7	Entas_2592	Entas_2592-2596	AEN65322.1	AEN65323.1	AEN65324.1 AEN65325.1 AEN65321.1	<i>Enterobacter asburiae</i> LF7a	γ Proteobacteria	An opportunistic pathogen	CP003026
8	ETA_04540	ETA_04540-04580	CAO95501.1	CAO95502.1	CAO95503.1 CAO95504.1 CAO95500.1	<i>Erwinia tasmaniensis</i> strain ET1/99	γ Proteobacteria	Non-phytopathogenic strain. Isolated from apple flowers.	CU468135
9	PP4_34580	PP4_34580-34640	BAN55312.1	BAN55313.1	BAN55314.1 BAN55315.1 BAN55316.1	<i>Pseudomonas putida</i> NBRC 14164 DNA	γ Proteobacteria	Saprotrophic soil bacterium	AP013070

					BAN55317.1 BAN55311.1				
10	YE1856	YE1856-1861	CAL11936.1	CAL11937.1	CAL11938.1 CAL11939.1 CAL11940.1 CAL11935.1	<i>Yersinia enterocolitica</i> subsp. <i>enterocolitica</i> 8081	γ Proteobacteria	Causes infections in humans that usually lead to mild self-limiting enterocolitis or terminal ileitis and adenitis	AM286415
11	Pput_3332	Pput_3332-3338	ABQ79459.1	ABQ79460.1	ABQ79461.1 ABQ79462.1 ABQ79463.1 ABQ79464.1 ABQ79458.1	<i>Pseudomonas putida</i> F1	γ Proteobacteria	A versatile environmental isolate that is capable of growth on several aromatic hydrocarbons	CP000712
12	PSEEN3394	PSEEN3394-3400	CAK16145.1	CAK16146.1	CAK16147.1 CAK16148.1 CAK16149.1 CAK16150.1 CAK16144.1	<i>Pseudomonas entomophila</i> str. L48 chromosome	γ Proteobacteria	Entomopathogenic bacterium which, upon ingestion, kills <i>Drosophila melanogaster</i>	CT573326
13	H045_11630	H045_11630-11660	AGE26392.1	AGE26393.1	AGE26394.1 AGE26395.1 AGE26396.1 AGE26397.1 AGE26391.1	<i>Pseudomonas poae</i> RE*1-1-14	γ Proteobacteria	The endophytic bacterium shows broad antagonistic activity and is applied to seeds as a biocontrol agent to suppress late root rot in the sugar beet	CP004045
14	M634_16975	M634_16975-16995	AGQ93894.1	AGQ92617.1	AGQ92618.1 AGQ92619.1 AGQ92616.1	<i>Vibrio parahaemolyticus</i> O1:Kuk str. FDA R31 chromosome II	γ Proteobacteria	A pathogenic marine bacterium that is the main causative agent of bacterial seafood-borne gastroenteritis in the United States	CP006005
15	PFL_3949	PFL_3955-3949	AAY93214.1	AAY93215.1	AAY93213.1 AAY93216.1 AAY93217.1 AAY93218.1 AAY93219.2	<i>Pseudomonas fluorescens</i> Pf-5	γ Proteobacteria	Pathogenic bacterium, usually affects patients with compromised immune systems	CP000076
16	PAGR_g0744	PAGR_g0744-g0749	AER31282.1	AER31283.1	AER31284.1 AER31285.1 AER31280.1	<i>Pantoea ananatis</i> PA13	γ Proteobacteria	Plant pathogen. Isolated from a diseased rice grain.	CP003085
17	EbC_38210	EbC_38170-38210	CAX61351.1	CAX61350.1	CAX61352.1 CAX61349.1 CAX61348.1	<i>Erwinia billingiae</i> strain Eb661	γ Proteobacteria	An epiphytic bacteria and may represent antagonists for biocontrol of fire blight	FP236843
18	ESA_01347	ESA_01343-01347	ABU76606.1	ABU76605.1	ABU76607.1 ABU76604.1 ABU76603.1	<i>Cronobacter sakazakii</i> ATCC BAA-894	γ Proteobacteria	Human pathogen. Enterobacter infection.	CP000783
19	ROD_19341	ROD_19341-19381	CBG88687.1	CBG88688.1	CBG88689.1 CBG88690.1 CBG88686.1	<i>Citrobacter rodentium</i> ICC168	γ Proteobacteria	Cause enteric disease with a high rate of fatality in mice and other rodents	FN543502
20	ECENHK_13825	ECENHK_13825-13845	AFP70615.1	AFP70616.1	AFP70614.1 AFP70618.1	<i>Enterobacter cloacae</i> subsp. <i>cloacae</i> ENHUKU01	γ Proteobacteria	Nosocomial pathogen	CP003737
21	Acav_4532	Acav_4528-4532	ADX48414.1	ADX48413.1	ADX48411.1 ADX48412.1 ADX48415.1	<i>Acidovorax avenae</i> subsp. <i>avenae</i> ATCC 19860	β Proteobacteria	Causes seedling blight and bacterial fruit blotch of cucurbits. Under favorable environment, it becomes devastating and may cause 100% loss of marketable fruit.	CP002521
22	BMASAVP1_A1401	BMASAVP1_A1395-A1401	ABM52929.1	ABM52936.1	ABM52947.1 ABM50447.1 ABM50929.1 ABM50824.1	<i>Burkholderia mallei</i> SAVP1 chromosome I	β Proteobacteria	A phenotypic avirulent strain	CP000526

23	<i>BPC006_I168_2</i>	<i>BPC006_I1677-I1682</i>	<u>AFR15557.1</u>	<u>AFR15556.1</u>	<u>AFR15558.1</u> <u>AFR15555.1</u> <u>AFR15554.1</u> <u>AFR15553.1</u>	<i>Burkholderia pseudomallei BPC006 chromosome I</i>	β <i>Proteobacteria</i>	Isolated from a melioidosis patient	CP00378
24	<i>MDS_2712</i>	<i>MDS_2707-2712</i>	<u>AEB58742.1</u>	<u>AEB58741.1</u>	<u>AEB58743.1</u> <u>AEB58740.1</u> <u>AEB58739.1</u> <u>AEB58738.1</u>	<i>Pseudomonas mendocina NK-01</i>	γ <i>Proteobacteria</i>	Isolated from farmland soil	CP002620
25	<i>YPC_2125</i>	<i>YPC_2119-2125</i>	<u>ADV98708.1</u>	<u>ADV98707.1</u>	<u>ADV98710.1</u> <u>ADV98706.1</u> <u>ADV98705.1</u> <u>ADV98704.1</u>	<i>Yersinia pestis biovar Medievalis str. Harbin 35</i>	γ <i>Proteobacteria</i>	Causative agent of bubonic and pneumonic plague	CP001608
26	<i>SMWW4_vlc2_1200</i>	<i>SMWW4_vlc21200-vlc21250</i>	<u>AGE17922.1</u>	<u>AGE17923.1</u>	<u>AGE17924.1</u> <u>AGE17925.1</u> <u>AGE17926.1</u> <u>AGE17921.1</u>	<i>Serratia marcescens WW4</i>	γ <i>Proteobacteria</i>	A biofilm-forming bacterium isolated from paper machine aggregates	CP003959
27	<i>ECA3077</i>	<i>ECA3073-3076</i>	<u>CAG75975.1</u>	<u>CAG75974.1</u>	<u>CAG75972.1</u> <u>CAG75973.1</u> <u>CAG75976.1</u>	<i>Erwinia carotovora subsp. Atroseptica SCR11043</i>	γ <i>Proteobacteria</i>	Plant pathogenic bacterium, the causative agent of soft rot and blackleg potato diseases	BX950851
28	<i>NCGM2_0934</i>	<i>NCGM2_0934-0939</i>	<u>BAK87811.1</u>	<u>BAK87812.1</u>	<u>BAK87813.1</u> <u>BAK87814.1</u> <u>BAK87815.1</u> <u>BAK87810.1</u>	<i>Pseudomonas aeruginosa NCGM2.SI DNA</i>	γ <i>Proteobacteria</i>	The multidrug-resistant strain that caused an outbreak of urinary tract infection	AP012280
29	<i>CsuE</i>	<i>Ab_Csu(A/B) ABCDE</i>	<u>AAP43039.1</u>	<u>AAP43038.1</u>	<u>AAP43035.1</u> <u>AAP43036.1</u> <u>AAP43037.1</u> <u>AAP43040.1</u>	<i>Acinetobacter baumannii 19606</i>	γ <i>Proteobacteria</i>	Pneumonia, meningitis, septicemia, and urinary and respiratory tract infections in immuno-compromised individuals	AY241696
30	<i>BJAB0868_0454</i>	<i>BJAB0868_02454-02459</i>	<u>AGQ11004.1</u>	<u>AGQ11005.1</u>	<u>AGQ11006.1</u> <u>AGQ11003.1</u> <u>AGQ11008.1</u>	<i>Acinetobacter baumannii BJAB0868</i>	γ <i>Proteobacteria</i>	Clinical isolate	CP003849
31	<i>A3UG_03070</i>	<i>A3UG_03070-0-03085</i>	<u>AFM58362.1</u>	<u>AFM58363.1</u>	<u>AFM58364.1</u> <u>AFM58361.1</u>	<i>Enterobacter cloacae subsp. dissolvens SDM</i>	γ <i>Proteobacteria</i>	Isolated from soil samples	CP003678
32	<i>P795_6510</i>	<i>P795_6495-6510</i>	<u>AHB91026.1</u>	<u>AHB91025.1</u>	<u>AHB91027.1</u> <u>AHB91024.1</u>	<i>Acinetobacter baumannii ZW85-1</i>	γ <i>Proteobacteria</i>	Isolated from diarrheal patient feces	CP006768
33	<i>PSYCG_09745</i>	<i>PSYCG_09730-09745</i>	<u>AGP49448.1</u>	<u>AGP49447.1</u>	<u>AGP49449.1</u> <u>AGP49446.1</u>	<i>Psychrobacter sp. G</i>	γ <i>Proteobacteria</i>	Nonpathogenic soil bacterium, isolated from King George Island, Antarctica	CP006265
34	<i>XCC1378</i>	<i>XCC1381-1376</i>	<u>AAM40677.1</u>	<u>AAM40674.1</u> <u>AAM40678.1</u>	<u>AAM40676.1</u> <u>AAM40679.1</u>	<i>Xanthomonas campestris str. ATCC 33913</i>	γ <i>Proteobacteria</i>	Causes a variety of plant disease	NC_003902
35	<i>XAC1424</i>	<i>XAC1427-1423</i>	<u>AAM36296.1</u>	<u>AAM36294.1</u> <u>AAM36297.1</u>	<u>AAM36295.1</u> <u>AAM36298.1</u>	<i>Xanthomonas axonopodis pv. citri str. 306</i>	γ <i>Proteobacteria</i>	Exclusively pathogenic to a large group of plants such as citrus trees, rice, cotton, beans, and grapes	NC_003919
36	<i>VAPA_1c2056_0</i>	<i>VAPA_1c2056-60-1c20590</i>	<u>AGU49161.1</u>	<u>AGU49162.1</u>	<u>AGU49163.1</u> <u>AGU49160.1</u>	<i>Variovorax paradoxus B4 chromosome 1</i>	β <i>Proteobacteria</i>	Degradates the organic thiol compound mercaptosuccinate, which could be a promising precursor for novel polythioesters	CP003911
37	<i>Sinme_6943</i>	<i>Sinme_6940-6943</i>	<u>AEG58265.1</u>	<u>AEG58264.1</u>	<u>AEG58266.1</u> <u>AEG58263.1</u>	<i>Sinorhizobium meliloti AK83 plasmid pSINME02</i>	α <i>Proteobacteria</i>	Plant endosymbiont	CP002785
38	<i>Bcep18194_A_5756</i>	<i>Bcep18194_A5756-A5759</i>	<u>ABB09353.1</u>	<u>ABB09352.1</u>	<u>ABB09350.1</u> <u>ABB09351.1</u>	<i>Burkholderia sp. 383 chromosome 1</i>	β <i>Proteobacteria</i>	Isolated from forest soil	CP000151
39	<i>Mesop_1922</i>	<i>Mesop_1919</i>	<u>AEH86402.1</u>	<u>AEH86401.1</u>	<u>AEH86403.1</u>	<i>Mesorhizobium</i>	α <i>Proteobacteria</i>	Isolated from B.	CP002279

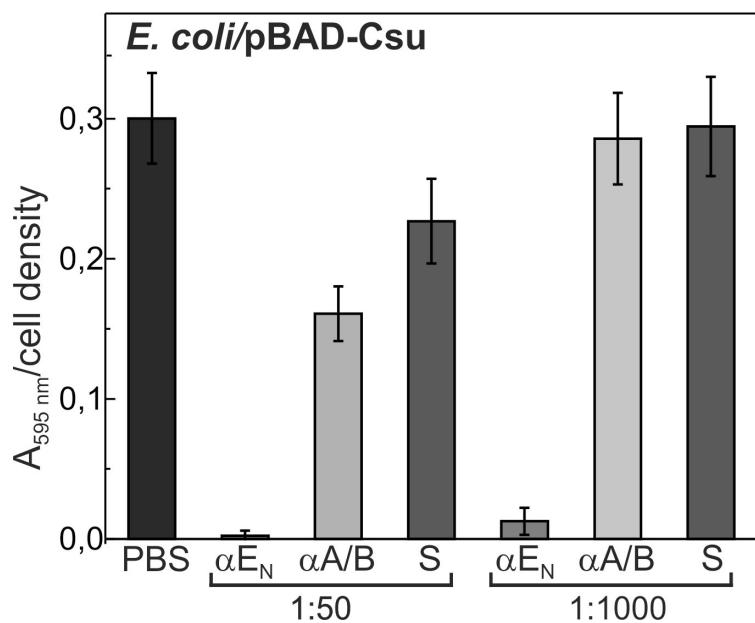
		1922			AEH86400.1	<i>opportunistum</i> <i>WSM2075</i>		pelecinus plants	
40	<i>BBK_506</i>	<i>BBK_506-</i> 509	AGZ27361.1	AGZ28430.1	AGZ28097.1 AGZ29774.1	<i>Burkholderia</i> <i>pseudomallei</i> <i>NCTC 13179</i> <i>chromosome 1</i>	β <i>Proteobacteria</i>	Human pathogen. Melioidosis.	CP003976
41	<i>Rta_34890</i>	<i>Rta_34850-</i> 34890	AEG94601.1	AEG94600.1	AEG94602.1 AEG94599.1	<i>Ramlibacter</i> <i>tataouinensis</i> <i>TTB310</i>	β <i>Proteobacteria</i>	Isolated in the Tataouine meteorite in the desert of South Tunisia	CP000245
42	<i>BYI23_D0121_10</i>	<i>BYI23_D012</i> 120- <i>D012150</i>	AET94722.1	AET94723.1	AET94721.1 AET94724.1	<i>Burkholderia</i> sp. <i>Y123 plasmid</i> <i>byi_1p</i>	β <i>Proteobacteria</i>	Isolated from a golf course soil	CP003090
43	<i>ABO_0699</i>	<i>ABO_0702-</i> 0699	CAL16149.1	CAL16148.1	CAL16147.1 CAL16150.1	<i>Alcanivorax</i> <i>borkumensis</i>	γ <i>Proteobacteria</i>	Nonpathogenic marine bacterium	AM28669 0
44	<i>BRPE64_DCD_S03180</i>	<i>BRPE64_DC</i> DS03190- 03210	BAN27255.1	BAN27256.1	BAN27257.1 BAN27254.1	<i>Burkholderia</i> sp. <i>RPE64 plasmid</i> <i>p1 DNA</i>	β <i>Proteobacteria</i>	Isolated from field- collected <i>Riptortus</i> <i>pedestris</i>	AP013061
45	<i>AXYL_05495</i>	<i>AXYL_05492</i> -05495	ADP18794.1	ADP18793.1	ADP18792.1 ADP18795.1	<i>Achromobacter</i> <i>xylosoxidans</i> A8	β <i>Proteobacteria</i>	Isolated from soil contaminated with polychlorinated biphenyls.	CP002287
46	<i>Smlt1510</i>	<i>Smlt1508-</i> 1513	CAQ45047.1	CAQ45048.1 AQ45044.1	CAQ45049.1 CAQ45046.1	<i>Stenotrophomonas</i> <i>malophilia</i> <i>K279a</i>	γ <i>Proteobacteria</i>	Human pathogen isolated from a patient undergoing chemotherapy developed a bloodstream infection that did not respond to therapy with piperacillin/tazobactam, ceftazidime or imipenem	AM74316 9
47	<i>OA238_c4625_0</i>	<i>OA238_c462</i> 10-c46250	AGI74478.1	AGI74477.1	AGI74479.1 AGI74475.1	<i>Octadecabacter</i> <i>arcticus</i> 238	α <i>Proteobacteria</i>	Isolated from sea ice of the Arctic	CP003742 1
48	<i>Entcl_2278</i>	<i>Entcl_2275-</i> 2278	ADO48529.1	ADO48528.1	ADO48527.1 ADO48530.1	<i>Enterobacter</i> <i>lignolyticus</i> <i>SCF1</i>	γ <i>Proteobacteria</i>	Isolated anaerobically from tropical forest soils	CP002272
49	<i>XOO1979</i>	<i>XOO1982-</i> 1978	AAW75234.1	AAW75232.1 AAW75235.1	AAW75233.1 AAW75236.1	<i>Xanthomonas</i> <i>oryzae</i> pv. <i>oryzae</i> <i>KACC10331</i>	γ <i>Proteobacteria</i>	Causes bacterial blight of rice	AE013598

Fig. S12

MNIKTKLLRHLCMSGLMLTGNMAHAACSVSASGTSSISVPSIYLMENGENSSQFNSGLSCTGF
SLALANMTYLKYRVEQMSNSFTNAQTGEKLNAAIILDSNNEIIISLGQEKDMSSTLVNLFGSPDGN
LPFYIRLPAGQSVSPGVYQADSPLKVWFYSVPAVAIVGIGVFFESPGFRRGALGIGFNWGSGAD
SLGSLSITVLPDHHHHHH

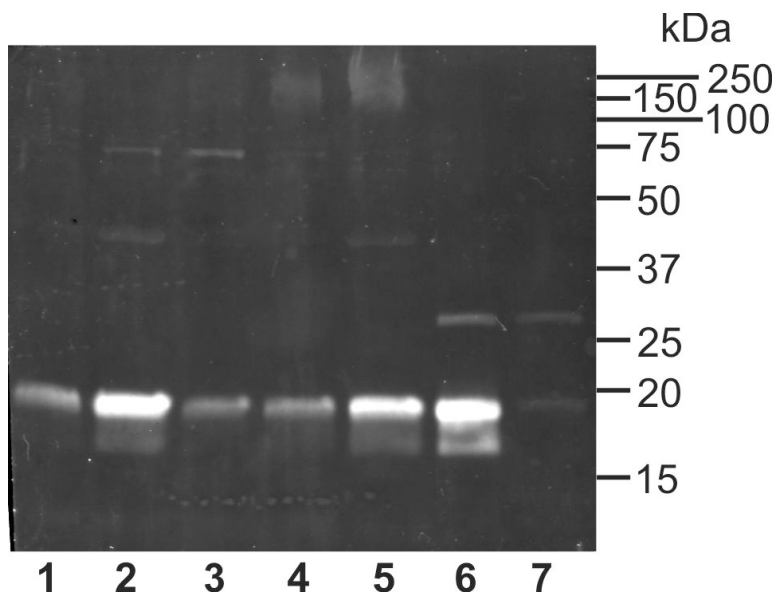
Protein sequence of N-terminal domain of CsuE tagged with six histidine residues. Signal peptide and His₆-tag are shown in blue and green, respectively.

Fig. S13



Anti-CsuE antibody blocks Csu-pili mediated biofilm formation. *E. coli*/pBAD-Csu cells overexpressing Csu pili were preincubated with PBS buffer, 1:50 and 1:1000 dilutions of antibodies raised against the N-terminal domain of CsuE (αE_N) and CsuA/B ($\alpha A/B$) or the preimmune serum (S) and then assayed for biofilm formation in polystyrene microtiter plates. Biofilms were quantified by crystal violet staining and measuring absorbance at 595 nm. The results are representative of three independent experiments.

Fig. S14



Csu pili are constitutively expressed and assembled on the cell surface of different *Acinetobacter baumannii* strains. Surface extracts prepared from *A. baumannii* strains 59798, 60611, 68164, 890, and 19069T from the Culture Collection of the University of Gothenburg (CCUG), lanes 1-5, respectively, and *E. coli* BL21 harboring pBAD-Csu in the presence (lane 6) and absence (lane 7) of arabinose, inducing Csu pili expression, were analyzed by Western blotting. The blot was probed with anti-CsuA/B rabbit serum followed by detection with IRDye 68RD-conjugated goat anti-rabbit antibody. The mobility of molecular mass markers is shown to the right in the figure.

Table S1.**Strains**

<i>Escherichia coli</i>						
BL21-AI	<i>E. coli</i> strain B F ⁻ <i>ompT gal dcm lon hsdS_B(r_B⁻m_B⁻) [malB⁺]K-12(λ^S) araB::T7RNAP-tetA</i>					
<i>Acinetobacter baumannii</i>						
Strain ^a	Source	Country	Year	Csu pili expression level ^b	Anti-CsuE serum dilution required for biofilm inhibition ^c	
CCUG 19096 T	Urine	France	1986	+++	1:1000	
CCUG 60611	Blood	Netherlands	1997	+++	1:1000	
CCUG 68164	Abdomen	Sweden	2006	++	1:1000	
CCUG 59798	Urine	Sweden	2010	+	1:1000	
CCUG 890	Urine	Great Britain	1970	+	1:1000	

^a All strains were from the Culture Collection, University of Gothenburg (CCUG)^b Estimated from the intensity of the band of CsxA/B in Western blots (Fig. S14)^c Example of the experiment is shown in Fig. 4.

Table S2.
Oligonucleotides

Name	Sequence (5'→3')
CsuABCDE_N-F	AAGCGGCCGCAGATTGCCATATTTATTCGAG
CsuABCDE_S-R	TTGAGCTCTTAAAGATAAAAGCCATGAACGTGAG
Δ-CsuAB-R	GAATTCCGTTAACCTCCTGTTAG
Δ-CsuAB-F	GAGTAGCAGGTTGCTCAAATATG
Δ-CsuA-R	TTAGAAATTACAGTGACTAATAGAGTATC
Δ-CsuA-F	TAGTACCAATTACGATTGAGTTTAAG
Δ-CsuB-R	TTTCTTAAACTCAATCGTAATTGGTAC
Δ-CsuB-F	ACGGCCGGAATTATAAAGATACTG
Δ-CsuE-R	TCATGGCAAAGATACTCGTGA
Δ-CsuE-F	TAAAAGCTGTTTATATAGGAGATAAAAG
CsuE-LALA_R	ACCCGAGCTAAAACCCGTACACGACAAAC
CsuE-LALA_F	TCAGGAAACATGACCTACCTAAAATATCGGGTTG
CsuE-IVGIGV_R	TCCCGAACTCGCGACTGCGGGCACAGAATAG
CsuE-IVGIGV_F	AGCGGGTCGTTCTTGAGAGTCCTGGGTTAG
CsuE-LGI_R	CCAATGCACCGCGTCTAAACCCAGG
CsuE-LGI_F	GTATTGGTTTAACTGGGGAAAGTGGGGC
CsuEN6Hrev	GTGATGATGAAGTACGGTAATTGAGAGTGAAC
CsuEN6Hfwd	CATCACCATTAAATGAAAGGGCGAGCTC
CsuE-N6H_PR	TGGAAGTACGGTAATTGAGAGTGAAC
CsuE-N6H_DF	GACCATCATCACCATCACCATTAATG

Table S3
Refinement statistics

Data set	Native data
Resolution	53.9-2.31
Number of reflections	
- Total	87930
- Work set	83189
- Test set	4741
R_{work}/R_{free} (%)	21.18/25.87
Number of atoms	
- Protein	7688
- Solvent	178
Number of protein residues	1000
Number of modified residues	6 (N-dimethyllysine) ^a
Number of ligands/ions	0
Wilson B-factor (Å²)	54.01
Average B-factor (Å²)	
- Main chain	65.77
- Side chain	78.15
- Solvent	55.20
Rmsd stereochemistry	
- Bond lengths (Å)	0.0043
- Bond angles (°)	1.050
Rmsd B-factors	
- Main chain	4.106
- Side chain	4.982
Ramachandran analysis^b	
Residues in outlier regions	0.73%
Residues in favored regions	95.7%
Residues in allowed regions	99.27%

^a Methylated lysine residues

^b Output from Molprobity (outliers motivated by electron density)

SI References

1. Pakharukova N, *et al.* (2016) Structural basis for Myf and Psa fimbriae-mediated tropism of pathogenic strains of Yersinia for host tissues. *Mol Microbiol* 102(4):593-610.
2. Pakharukova N, Tuittila M, Paavilainen S, & Zavialov A (2017) Methylation, crystallization and SAD phasing of the Csu pilus CsuC-CsuE chaperone-adhesin subunit pre-assembly complex from *Acinetobacter baumannii*. *Acta crystallographica. Section F, Structural biology communications* 73(Pt 8):450-454.
3. Pakharukova N, Tuittila M, Paavilainen S, & Zavialov A (2015) Crystallization and preliminary X-ray diffraction analysis of the Csu pili CsuC-CsuA/B chaperone-major subunit pre-assembly complex from *Acinetobacter baumannii*. *Acta crystallographica. Section F, Structural biology communications* 71(Pt 6):770-774.
4. Emsley P, Lohkamp B, Scott WG, & Cowtan K (2010) Features and development of Coot. *Acta Crystallogr D Biol Crystallogr* 66(Pt 4):486-501.
5. Le Trong I, *et al.* (2010) Structural basis for mechanical force regulation of the adhesin FimH via finger trap-like beta sheet twisting. *Cell* 141(4):645-655.
6. Pakharukova N, *et al.* (2015) Structural Insight into Archaic and Alternative Chaperone-Usher Pathways Reveals a Novel Mechanism of Pilus Biogenesis. *PLoS Pathog* 11(11):e1005269.
7. Bork P, Holm L, & Sander C (1994) The immunoglobulin fold. Structural classification, sequence patterns and common core. *J. Mol. Biol.* 242(4):309-320.
8. Holm L & Rosenstrom P (2010) Dali server: conservation mapping in 3D. *Nucleic Acids Res* 38(Web Server issue):W545-549.
9. Li YF, *et al.* (2007) A receptor-binding site as revealed by the crystal structure of CfaE, the colonization factor antigen I fimbrial adhesin of enterotoxigenic *Escherichia coli*. *J Biol Chem* 282(33):23970-23980.
10. Sievers F, *et al.* (2011) Fast, scalable generation of high-quality protein multiple sequence alignments using Clustal Omega. *Mol Syst Biol* 7.
11. Waterhouse AM, Procter JB, Martin DM, Clamp M, & Barton GJ (2009) Jalview Version 2—a multiple sequence alignment editor and analysis workbench. *Bioinformatics* 25(9):1189-1191.